Acta Mech. Sin. (2011) 27(6):898–910
DOI 10.1007/s10409-011-0469-1

RESEARCH PAPER

Effects of bottom shear stresses on the wave-induced dynamic response in a porous seabed: PORO–WSSI (shear) model

J. Ye · D.-S. Jeng

Received: 16 July 2010 / Revised: 17 January 2011 / Accepted: 4 March 2011

Abstract When ocean waves propagate over the sea floor, dynamic wave pressures and bottom shear stresses exert on the surface of seabed. The bottom shear stresses provide a horizontal loading in the wave-seabed interaction system, while dynamic wave pressures provide a vertical loading in the system. However, the bottom shear stresses have been ignored in most previous studies in the past. In this study, the effects of the bottom shear stresses on the dynamic response in a seabed of finite thickness under wave loading will be examined, based on Biot's dynamic poro-elastic theory. In the model, an "*u*–*p*" approximation will be adopted instead of quasi-static model that have been used in most previous studies. Numerical results indicate that the bottom shear stresses has certain influences on the wave-induced seabed dynamic response. Furthermore, wave and soil characteristics have considerable influences on the relative difference of seabed response between the previous model (without shear stresses) and the present model (with shear stresses). As shown in the parametric study, the relative differences between two models could up to 10% of p_0, depending on the amplitude of bottom shear stresses.

Keywords Bottom shear stresses · Wave-induced dynamic response · Porous seabed · "*u*–*p*" approximation · Biot's theory

D.-S. Jeng (✉)
Center for Marine Geotechnical Engineering,
State Key Laboratory of Ocean Engineering,
Shanghai Jiao Tong University,
200240 Shanghai, China
e-mail: d.jeng@dundee.ac.uk; d.jeng@sjtu.edu.cn

J. Ye · D.-S. Jeng
Division of Civil Engineering,
University of Dundee, DD1 4HN, UK

1 Introduction

The evaluation of the wave-induced dynamic response in a porous seabed is particularly important for coastal geotechnical engineers involved in the design of the foundations of marine structures. An inappropriate design and maintenance of the foundation around a marine structure would result in the disastrous failure of structures. Numerous failures of marine structures due to the liquefaction or shear failure of seabed have been reported in Refs. [1–5].

Based on Biot's poro-elastic theory [6,7], numerous investigations of the wave-induced dynamic response of a porous seabed under wave loading have been carried out since the 1970s. Among these, Yamamoto et al. [8] derived an analytical solution for an isotropic, poro-elastic infinite seabed by treating the pore water and seabed as compressible and deformable medium. Later, Hsu and Jeng [9] further derived an analytical solution for an unsaturated, isotropic seabed with finite thickness under three-dimensional short-crested waves loading. Such a model has been further extended to a layered seabed [10], non-homogeneous seabed such as variable permeability and shear modulus [11–13], cross-anisotropic seabed [14] or non-linear wave loading [15]. A detailed review of previous relevant research can be found in Ref. [16]. More recenly, another analytical approximation, transmission and reflection matrices (TRM), was proposed to handle the multi-layered porous seabed due to wave loading [17].

To simplify the problem of wave-seabed interaction, most previous investigations considered the dynamic wave pressures along the seabed surface as the only external loading, and ignored the bottom shear stresses which are horizontal external loading. Sakai et al. [18] may have been the first to consider the bottom shear stresses in the problem of the wave-seabed interaction, based on a boundary layer approximation. In their model, the bottom shear stresses are as-

sumed having the same phase with the ocean waves, which in fact has a 45° phase lag, according to the boundary layer theory [19]. Therefore, the Sakai's results are doubtful. Later, Jeng [20] derived a simple analytical solution for the wave-induced soil response with the correct phase of bottom shear stresses, but only limited to infinite seabed and quasi-static Biot's consolidation theory.

It is noted that most existing porous models for the wave-induced soil response have been limited to quasi-static soil model. That is, the acceleration of soil particles and pore fluid have been ignored. If the acceleration of pore fluid and solid particles are taken into account, a so-called "*u–p*" approximation was proposed [21]. The ranges of applications of the quasi-static, "*u–p*" approximation and full dynamic models versus different wave and soil characteristics have been discussed and clarified in the recent publications [22,23]. However, the effect of bottom shear stresses on the dynamic response under wave loading have not been considered, although it is expected to have certain influences in the evaluation of the wave-induced seabed response.

In this study, the existing finite element model (SWANDYNE II), originally developed for earthquake loading [24,25], will be implemented for wave loading with bottom shear stresses, and integrated into the PORO-WSSI (porous model for wave-seabed-structure interactions) model [26]. The bottom shear stresses along the seabed surface are included in the existing poro-elastic model as a horizontal loading, together with the dynamic wave pressures as the vertical loading. The dynamic Biot's poro-elastic theory [7], instead of the conventional quasi-static Biot's consolidation equations [20], are adopted in this study. With this new model, the influences of bottom shear stresses on the wave-induced pore pressure are also examined through a parametric study.

2 Boundary value problem

2.1 Wave field

Based on the second-order Stokes wave theory, the free surface elevation (η) and dynamic pressure acting on seabed (P_b) can be expressed as

$$\eta(x,t) = \frac{H}{2}\cos(kx-\omega t) + \frac{\pi H^2}{8L} \times \frac{\cosh(kd)[2+\cosh(2kd)]}{\sinh^3(kd)}\cos 2(kx-\omega t), \quad (1)$$

$$P_b(x,t) = \frac{\rho g H}{2\cosh(kd)}\cos(kx-\omega t) + \frac{3\pi\rho g H^2}{8L} \times \frac{\tanh(kd)}{\sinh^2(kd)}\left[\frac{1}{\sinh^2(kd)} - \frac{1}{3}\right]\cos 2(kx-\omega t), \quad (2)$$

where H is the wave height, $\omega = 2\pi/T$ is the angular frequency and T is the wave period, d is the water depth and k is the wave number. The wave dispersion relation is given as

$$\omega^2 = gk\tanh(kd). \quad (3)$$

With the second-order Stokes wave theory, the bottom shear stress can be derived from the boundary layer theory up the second-order, which can be expressed as [27]

$$\tau_b(x,t) = -\frac{\beta_2\rho\nu}{\delta} + \frac{\sqrt{2}\beta_0\rho\nu kH}{2\delta}\cos\left(kx-\omega t-\frac{\pi}{4}\right) + \frac{4\rho\nu}{\delta}[ka^2\beta_1 + (1-\sqrt{2})\beta_4]\cos 2\left(kx-\omega t-\frac{\pi}{8}\right), \quad (4)$$

where ρ is fluid density, ν is the kinematic viscosity of water, $\delta = \sqrt{2\nu/\omega}$, ω is the angular frequency of wave. The β_i coefficients ($i = 0, 1, 2$) are defined as

$$\beta_0 = \frac{\omega}{k\sinh(kd)}, \quad (5)$$

$$\beta_1 = \frac{3\omega}{8\sinh^4(kd)}, \quad (6)$$

$$\beta_2 = \frac{k^3a^2\beta_0^2}{4\omega}. \quad (7)$$

It is noted that Eqs. (2) and (4) represent the second-order solution of dynamic wave pressure and bottom shear stresses. For the linear wave theory, only the first term is required.

2.2 Governing equations

In this study, the seabed soil is considered as a porous medium comprised of soil particles and pore water. The Biot's poro-elastic theory [7] is commonly used to describe the mechanical behaviour of porous medium. Herein, the "*u–p*" approximation [21] for dynamic problems is adopted, in which the accelerations of the solid and pore fluid are considered. The forces equilibrium and the continuity equations are expressed as

$$\frac{\partial\sigma'_x}{\partial x} + \frac{\partial\tau_{xz}}{\partial z} = -\frac{\partial p}{\partial x} + \rho\frac{\partial^2 u}{\partial t^2}, \quad (8)$$

$$\frac{\partial\tau_{xz}}{\partial x} + \frac{\partial\sigma'_z}{\partial z} + \rho g = -\frac{\partial p}{\partial z} + \rho\frac{\partial^2 w}{\partial t^2}, \quad (9)$$

$$k\nabla^2 p - \gamma_w n\beta\frac{\partial p}{\partial t} + k\rho_f\frac{\partial^2\epsilon}{\partial t^2} = \gamma_w\frac{\partial\epsilon}{\partial t}, \quad (10)$$

where u and w are the soil displacements in the horizontal and vertical directions, respectively; n is soil porosity; σ'_x and σ'_z are effective normal stresses in the horizontal and vertical directions, respectively; τ_{xz} is shear stress; p is the pore water pressure; $\rho = \rho_f n + \rho_s(1-n)$ is the average density of porous seabed; ρ_f is the fluid density; ρ_s is solid density; k is the Darcy's permeability; g is the gravitational acceleration and ϵ is the volumetric strain. k_w is the wave number. In Eq. (10), the compressibility of pore fluid (β) and the volume strain (ϵ) are defined as

$$\beta = \left(\frac{1}{K_f} + \frac{1 - S_r}{p_{w0}}\right),$$
$$\epsilon = \frac{\partial u}{\partial x} + \frac{\partial w}{\partial z}, \tag{11}$$

where S_r is the degree of saturation of seabed, p_{w0} is the absolute static pressure and K_f is the bulk modulus of pore water.

In this study, poro-elastic soil behavior is considered as the first approximation, the stress–strain relation under plane strain conditions can be expressed as

$$\sigma'_x = 2G\left(\frac{\partial u}{\partial x} + \frac{\mu\epsilon}{1-2\mu}\right), \tag{12}$$

$$\sigma'_z = 2G\left(\frac{\partial w}{\partial z} + \frac{\mu\epsilon}{1-2\mu}\right), \tag{13}$$

$$\tau_{xz} = G\left(\frac{\partial u}{\partial z} + \frac{\partial w}{\partial x}\right), \tag{14}$$

where G is shear modulus; μ is Poisson's ratio.

Substituting Eqs. (12)–(14) into Eqs. (8) and (9), we have the expressions of force equilibrium as

$$G\nabla^2 u + \frac{G}{1-2\mu}\frac{\partial \epsilon}{\partial x} = -\frac{\partial p}{\partial x} + \rho\frac{\partial^2 u}{\partial t^2}, \tag{15}$$

$$G\nabla^2 w + \frac{G}{1-2\mu}\frac{\partial \epsilon}{\partial z} + \rho g = -\frac{\partial p}{\partial z} + \rho\frac{\partial^2 w}{\partial t^2}. \tag{16}$$

2.3 Boundary conditions

In this study, the dynamic wave pressures are adopted to apply the vertical loading, while the bottom shear stresses are the horizontal loading (Fig. 1). To solve the pore pressures and soil displacements in the governing equations (10), (15) and (16), appropriate boundary conditions are required.

It has been well-documented from that there is a 45° phase lag for the bottom shear stresses relative to the dynamic pressure acting on the seabed [19]. Then, the boundary condition at the surface of the seabed can be expressed as

$$p = P_b(x,t), \qquad \text{at } z = 0, \tag{17}$$

$$\tau_{xz} = \tau_b(x,t), \qquad \text{at } z = 0, \tag{18}$$

$$\sigma'_z = 0, \qquad \text{at } z = 0, \tag{19}$$

where γ_w is the unit weight of water, and P_b and τ_b are the dynamic wave pressures and bottom shear stresses, in which both linear and non-linear wave loadings can be considered.

Since the bottom boundary of the seabed is a rigid impermeable, the pore fluid can not enter the boundary and soil displacements will vanish, i.e.

$$u = v = 0, \qquad \frac{\partial p}{\partial n} = 0, \qquad \text{at } z = -h. \tag{20}$$

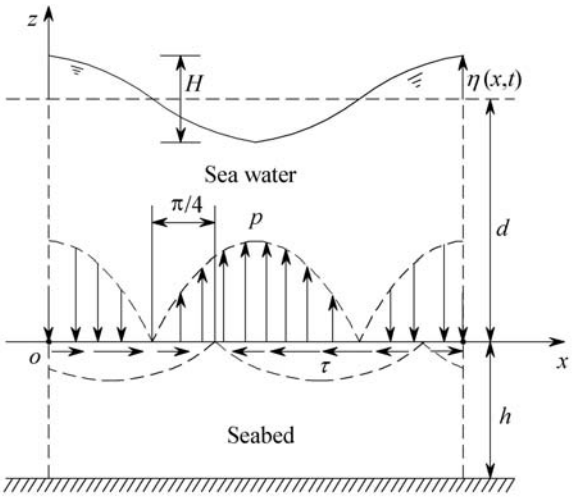

Fig. 1 The sketch of dynamic pressure and bottom shear stress acting on seabed when wave propagating over a porous seabed. The upward pressure is negative dynamic pressure. The leftward bottom shear stress is negative dynamic shear stress

In general, the periodic boundary conditions should be applied to the both lateral sides of computational domain due to that the computational domain is truncated from infinite (in the horizontal direction) seabed [28]. In the wave-seabed interaction poblem, the wave applied is periodic. Therefore, the horizontal and vertical displacement, and pore pressure at corresponding nodes on the two lateral sides exactly equal to each other at any time. However, the periodic boundary condition requires that the length of computational domain must be integer of the length of wave applied. This requirement may cause that different mesh systems have to be used in numerical calculation from cases to cases. In this study, a large computational domain is used, and the two lateral sides both are fixed in horizontal direction, the repetitive works of generation of mesh systems for different cases could then be avoided; because the influences of the two fixed lateral boundaries on the seabed response are only significant in the regions near them. The influences of the fixed lateral boundary conditions will disappear in the region far away from the two lateral boundaries. The feasibility and the accuracy of numerical results for adopting a large computational domain and fixed lateral boundary conditions will be further demonstrated in Sect. 3.2.

3 Numerical model

3.1 Finite element formulations

In this study, the finite element model (SWANDYNE II), originally developed for the soil response under earthquake loading [24], is adopted and a wave module with bottom shear stresses is developed and the integrated into the previous porous model (PORO–WSSI I) to form the PORO-WSSI (shear) model. In this section, the FEM formulations are out-

lined. For more detailed information, the readers can refer to Ref. [25].

The spatial discretization involves the variables $\boldsymbol{u}$ and $\boldsymbol{p}$ are replaced by suitable shape functions in the governing equations (10), (15) and (16).

$$\boldsymbol{u} = \sum N_i^u u_i = \boldsymbol{N}^u \overline{\boldsymbol{u}}, \qquad \boldsymbol{p} = \sum N_i^p p_i = \boldsymbol{N}^p \overline{\boldsymbol{p}}, \tag{21}$$

where $\boldsymbol{u}$ and $\boldsymbol{p}$ are the displacement vector of soil and the pore pressure. The $\overline{\boldsymbol{u}}$ and $\overline{\boldsymbol{p}}$ are the vectors of node displacement and pore pressure. The $\boldsymbol{N}^u$ and $\boldsymbol{N}^p$ are the shape function of displacement and pore pressure. The $\overline{\boldsymbol{u}}$, $\overline{\boldsymbol{p}}$, $\boldsymbol{N}^u$ and $\boldsymbol{N}^p$ are defined as

$$\overline{\boldsymbol{u}} = [u_1 \;\; w_1 \;\; u_2 \;\; w_2 \;\; \cdots \;\; u_n \;\; w_n]^{\mathrm{T}}, \tag{22}$$

$$\overline{\boldsymbol{p}} = [p_1 \;\; p_2 \;\; \cdots \;\; p_n]^{\mathrm{T}}, \tag{23}$$

$$\boldsymbol{N}^u = \begin{bmatrix} N_1^u & 0 & N_2^u & 0 & \cdots & N_n^u & 0 \\ 0 & N_1^u & 0 & N_2^u & \cdots & 0 & N_n^u \end{bmatrix}, \tag{24}$$

$$\boldsymbol{N}^{\boldsymbol{p}} = [N_1^p \;\; N_2^p \;\; \cdots \;\; N_n^p]. \tag{25}$$

Substituting Eqs. (21) into the governing equations (10), (15) and (16), and applying the minimum potential energy principle, the governing equations can be discretized in spatial domain as

$$\boldsymbol{M}\ddot{\overline{\boldsymbol{u}}} + \boldsymbol{K}\overline{\boldsymbol{u}} - \boldsymbol{Q}\overline{\boldsymbol{p}} = \boldsymbol{f}^{(1)}, \tag{26}$$

$$\boldsymbol{Q}^{\mathrm{T}}\ddot{\overline{\boldsymbol{u}}} + \boldsymbol{S}\dot{\overline{\boldsymbol{p}}} + \boldsymbol{H}\overline{\boldsymbol{p}} = \boldsymbol{f}^{(2)}, \tag{27}$$

$$\boldsymbol{M} = \int (\boldsymbol{N}^{\boldsymbol{u}})^{\mathrm{T}} \rho \boldsymbol{N}^u \mathrm{d}\Omega, \tag{28}$$

$$\boldsymbol{K} = \int \boldsymbol{B}^{\mathrm{T}} \boldsymbol{D} \boldsymbol{B} \mathrm{d}\Omega, \tag{29}$$

$$\boldsymbol{Q} = \int \boldsymbol{B}^{\mathrm{T}} m \boldsymbol{N}^p \mathrm{d}\Omega, \tag{30}$$

$$\boldsymbol{S} = \int (\boldsymbol{N}^{\boldsymbol{p}}) n\beta \boldsymbol{N}^p \mathrm{d}\Omega, \tag{31}$$

$$\boldsymbol{H} = \int (\boldsymbol{\nabla} \boldsymbol{N}^p)^{\mathrm{T}} k \boldsymbol{\nabla} \boldsymbol{N}^p \mathrm{d}\Omega, \tag{32}$$

$$\boldsymbol{\nabla} = \begin{bmatrix} \dfrac{\partial}{\partial x} \\ \dfrac{\partial}{\partial z} \end{bmatrix}, \tag{33}$$

$$\boldsymbol{B} = \begin{bmatrix} \dfrac{\partial}{\partial x} & 0 \\ 0 & \dfrac{\partial}{\partial z} \\ \dfrac{\partial}{\partial z} & \dfrac{\partial}{\partial x} \end{bmatrix} \boldsymbol{N}^u, \tag{34}$$

$$\boldsymbol{D} = \frac{E}{(1+\mu)(1-2\mu)} \begin{bmatrix} 1-\mu & \mu & 0 \\ \mu & 1-\mu & 0 \\ 0 & 0 & (1-2\mu)/2 \end{bmatrix}, \tag{35}$$

$$\boldsymbol{f}^{(1)} = \int (\boldsymbol{N}^u)^{\mathrm{T}} \rho \boldsymbol{g} \mathrm{d}\Omega + \int (\boldsymbol{N}^u)^{\mathrm{T}} \overline{\boldsymbol{t}} \mathrm{d}\Gamma, \tag{36}$$

$$\boldsymbol{f}^{(2)} = -\int (\boldsymbol{N}^p)^{\mathrm{T}} \boldsymbol{\nabla}^{\mathrm{T}} (k\rho_{\mathrm{f}} \boldsymbol{g}) \mathrm{d}\Omega + \int (\boldsymbol{N}^p)^{\mathrm{T}} \overline{\boldsymbol{q}} \mathrm{d}\Gamma, \tag{37}$$

where $\boldsymbol{m} = [1, 1, 1, 0, 0, 0]^{\mathrm{T}}$, $\overline{\boldsymbol{t}}$ is the stress acting on the surface of computational domain, $\overline{\boldsymbol{q}}$ is the pore water pressure on the surface of computational domain.

To complete the numerical solution, it is necessary to integrate the ordinary differential equations (26) and (27) in time domain. In the present model, the single-step Generalized Newmark (GN_{pj}) method [29,30] is employed. Using GN_{22} for the nodal displacements $\overline{\boldsymbol{u}}$, and GN_{11} for the nodal pore pressure $\overline{\boldsymbol{p}}$, the displacement, velocity and acceleration of nodes are written as

$$\ddot{\overline{\boldsymbol{u}}}_{n+1} = \ddot{\overline{\boldsymbol{u}}}_n + \Delta\ddot{\overline{\boldsymbol{u}}}_n, \tag{38}$$

$$\dot{\overline{\boldsymbol{u}}}_{n+1} = \dot{\overline{\boldsymbol{u}}}_n + \ddot{\overline{\boldsymbol{u}}}_n \Delta t + \beta_1^* \Delta\ddot{\overline{\boldsymbol{u}}}_n \Delta t, \tag{39}$$

$$\overline{\boldsymbol{u}}_{n+1} = \overline{\boldsymbol{u}}_n + \dot{\overline{\boldsymbol{u}}}_n \Delta t + \frac{1}{2}\ddot{\overline{\boldsymbol{u}}}_n \Delta t^2 + \frac{1}{2}\beta_2^* \Delta\ddot{\overline{\boldsymbol{u}}}_n \Delta t^2, \tag{40}$$

and the rate of pore pressure and the pore pressure are expressed as

$$\dot{\overline{\boldsymbol{p}}}_{n+1} = \dot{\overline{\boldsymbol{p}}}_n + \Delta\dot{\overline{\boldsymbol{p}}}_n, \tag{41}$$

$$\overline{\boldsymbol{p}}_{n+1} = \overline{\boldsymbol{p}}_n + \dot{\overline{\boldsymbol{p}}}_n \Delta t + \theta_1^* \Delta\dot{\overline{\boldsymbol{p}}}_n \Delta t. \tag{42}$$

In the above schemes, if the parameters β_1^*, β_2^* and θ_1^* satisfy following condition

$$\beta_2^* \geq \beta_1^* \geq \frac{1}{2}, \qquad \theta_1^* \geq \frac{1}{2}, \tag{43}$$

then, the GN_{pj} time integration scheme will be unconditional stable [24,25]. In this study, three parameters are choosen as: $\beta_2^* = 0.605$, $\beta_1^* = 0.6$ and $\theta_1^* = 0.6$, as suggested by Chan [24].

Substituting Eqs. (38)–(42) into Eqs. (26) and (27), leads to

$$\begin{bmatrix} \boldsymbol{M}_{n+1} + \dfrac{1}{2}\boldsymbol{K}_{n+1}\beta_2^* \Delta t^2 & -\boldsymbol{Q}_{n+1}\theta_1 \Delta t \\ \boldsymbol{Q}_{n+1}^{\mathrm{T}}\beta_1^* \Delta t & \boldsymbol{S}_{n+1} + \boldsymbol{H}_{n+1}\beta_1^* \Delta t \end{bmatrix} \begin{bmatrix} \Delta\ddot{\overline{\boldsymbol{u}}}_n \\ \Delta\dot{\overline{\boldsymbol{p}}}_n \end{bmatrix} = \begin{bmatrix} \boldsymbol{F}_{n+1}^{(1)} \\ \boldsymbol{F}_{n+1}^{(2)} \end{bmatrix}, \tag{44}$$

where the $\boldsymbol{F}_{n+1}^{(1)}$ and $\boldsymbol{F}_{n+1}^{(2)}$ are formulated as

$$\boldsymbol{F}_{n+1}^{(1)} = \boldsymbol{f}_{n+1}^{(1)} + \boldsymbol{Q}_{n+1}\overline{\boldsymbol{p}}_n + \boldsymbol{Q}_{n+1}\dot{\overline{\boldsymbol{p}}}_n \Delta t - \boldsymbol{M}_{n+1}\ddot{\overline{\boldsymbol{u}}}_n - \boldsymbol{K}_{n+1}\left(\overline{\boldsymbol{u}}_n + \dot{\overline{\boldsymbol{u}}}_n \Delta t + \frac{1}{2}\ddot{\overline{\boldsymbol{u}}}_n \Delta t^2\right), \tag{45}$$

$$\boldsymbol{F}_{n+1}^{(2)} = \boldsymbol{f}_{n+1}^{(2)} - \boldsymbol{S}_{n+1}\dot{\overline{\boldsymbol{p}}}_n - \boldsymbol{H}_{n+1}(\overline{\boldsymbol{p}}_n + \dot{\overline{\boldsymbol{p}}}_n \Delta t) - \boldsymbol{Q}_{n+1}(\dot{\overline{\boldsymbol{u}}}_n + \ddot{\overline{\boldsymbol{u}}}_n \Delta t). \tag{46}$$

In Eq. (44), the unknowns are $\Delta\ddot{\overline{\boldsymbol{u}}}_n$ and $\Delta\dot{\overline{\boldsymbol{p}}}_n$. At $n+1$ time step. They can be determined by solving Eq. (44) taking the values determined at n time step as the initial conditions. In this study, the Newton–Raphson method is adopted to solve Eq. (44). Once the incremental acceleration $\Delta\ddot{\overline{\boldsymbol{u}}}_n$ and incremental rate of pore pressure $\Delta\dot{\overline{\boldsymbol{p}}}_n$ are determined,

the displacement of soil and pore pressure can be accordingly obtained by applying Eqs. (40) and (42).

3.2 Treatments of lateral boundaries

As stated previously, in this study, a large computational domain is used, and the two lateral boundaries are fixed in horizontal direction. According to the Saint-Venant principle, the influence of the fixed lateral boundaries is only limited to the region near the lateral boundaries. In the region far away from the lateral boundaries, the influence of the fixed lateral boundaries will disappear. In this section, the feasibility and the accuracy of the numerical results in the region far away from the fixed lateral boundaries are demonstrated.

In general, a larger computational domain will reduce the effect of the fixed lateral boundaries. However, a large computation domain will cost more CPU running time and require larger memory. Therefore, in this study, the length of computation domain is chosen as 1.5 to 3.0 times of the maximum wave length adopted in all cases. A numerical example, with the input data (Table 1) and mesh (Fig.2), is illustrated in Fig. 3. In the numerical example, we consider a computational domain of 250 m long that is about 2.8 times of the wavelength (88.8 m). The results of applying the principle of repeatability [28] are also included for the comparison.

Table 1 Wave and soil characteristics used in numerical examples

	Characteristics	
Wave	Wave period T	8.0 s
	Wave height H_s	2.0 m
	Water depth d	20 m
	Wave length L	88.8 m
Soil	Permeability k	10 mm/s (coarse sand)
		0.1 mm/s (fine sand)
	Porosity n	0.3 (coarse sand)
		0.2 (fine sand)
	Shear modulus G	10 MPa
	Poisson's ratio μ	1/3
	Saturation S_r	0.98
	Thickness h	30 m

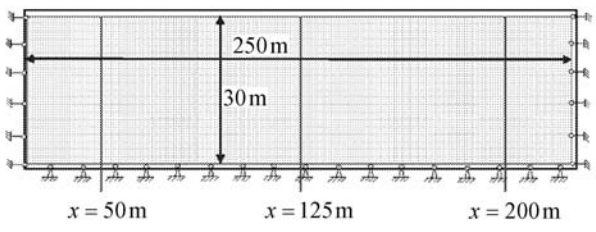

Fig. 2 Two lateral sides are fixed in horizontal direction in the mesh system used in this study

In this numerical example, three sections, $x = 50$ m, 125 m and 200 m are considered. To simplify the problem, linear wave theory is considered in this example. The sections of $x = 50$ m and 200 m are close to the lateral boundaries, while the section ($x = 125$ m) is far from both lateral boundaries. Two treatments of lateral boundary conditions are used here. First, the principle of repeatability [28] is used, and second, the fixed lateral boundary conditions are used. As shown in Figs. 3a and 3c, different treatments seem to slightly affect the results of pore pressure, and vertical effective stress only. However, the horizontal effective stress and shear stress are significantly different between two treatments. This indicates that the effects of a fixed lateral boundary are visible at these two sections. Figure 3b presents the comparison of the seabed response at the central section ($x = 125$ m). The figure clearly shows that the effect of the fixed lateral boundaries disappears completely at the region far away from the fixed lateral boundaries.

Based on the above numerical exercises, it can be concluded that the proposed treatment method for lateral boundaries is acceptable for the region near the center of computational domain. Therefore, the same mesh system is used for all cases in which different wave lengths are involved is feasible, and the accurate results could be obtained at the region far away from the fixed lateral boundaries, where is our main investigation zone.

3.3 Verifications

The finite element model, SWANDYNE II, was originally developed for investigating the earthquake-induced liquefaction in a saturated or unsaturated porous medium. To investigate the effect of bottom shear stresses on the wave-induced seabed response, a wave module is developed and integrated into the existing PORO-WSSI model and forms PORO-WSSI (shear) model. To verify the proposed numerical model, the model will compare with the previous analytical solution [9] and two sets of experimental data conducted by Lu [31].

3.3.1 Comparison with the analytical solution

Numerical results of the maximum values of wave-induced pore pressure and effective stresses in unsaturated coarse/fine sand (the degree of saturation is 98%) are shown in Fig. 4. The results of the analytical solution with linear wave loading but without bottom shear stresses [9] are also plotted in the figure. From Figs. 4a and 4b, it is found that the numerical solutions overall agree well with analytical solution. The minor differences between two models is because that the analytical solution was based on quasi-static soil behavior and the present model is based on "*u–p*" approximation.

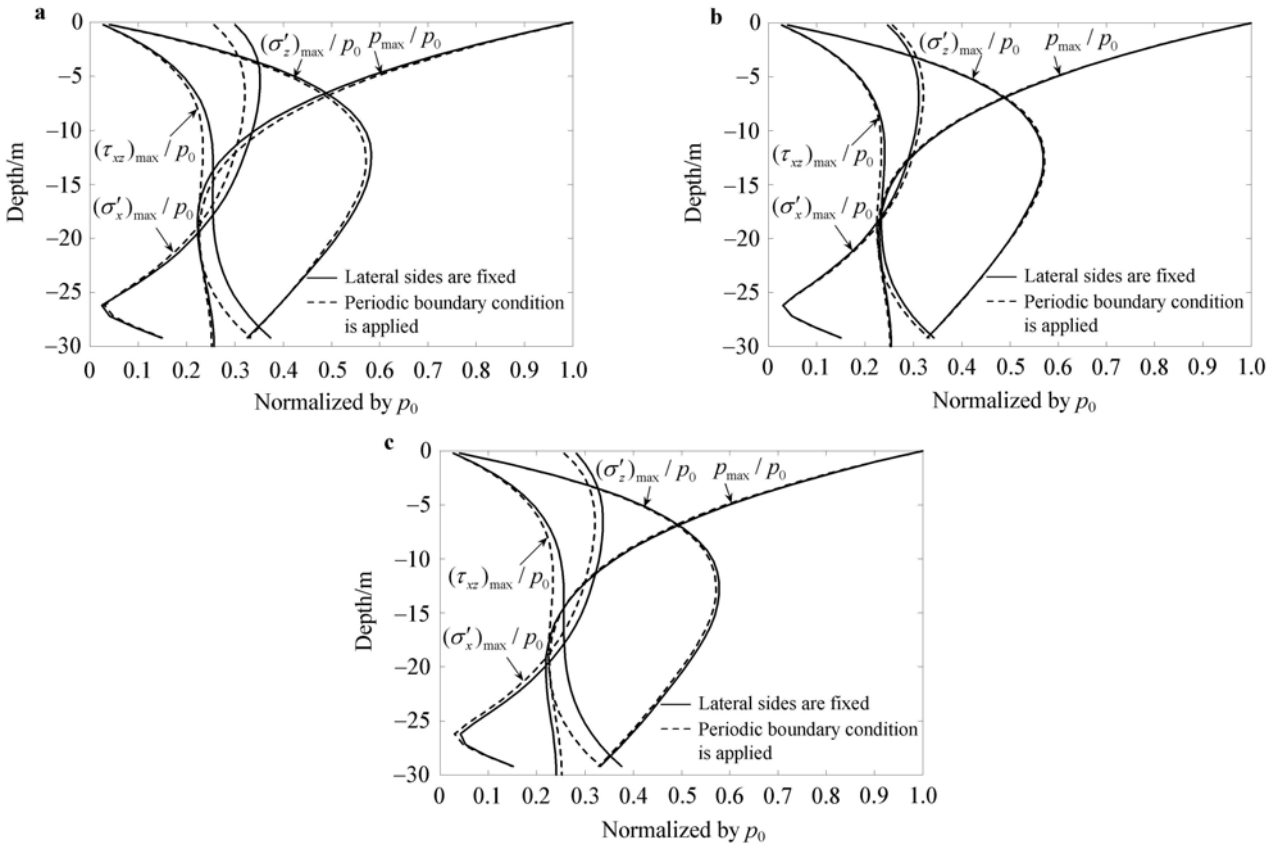

Fig. 3 Comparison of the seabed response with two different treatments of lateral boundary conditions. **a** $x = 50$ m; **b** $x = 125$ m; **c** $x = 200$ m. ($k = 0.01$ m/s, $T = 8.0$ s, $d = 20$ m, $L = 88.8$ m, $G = 10$ MPa, $\mu = 1/3$, $n = 0.3$, $S_r = 0.98$, $U_0 = 0$ m/s)

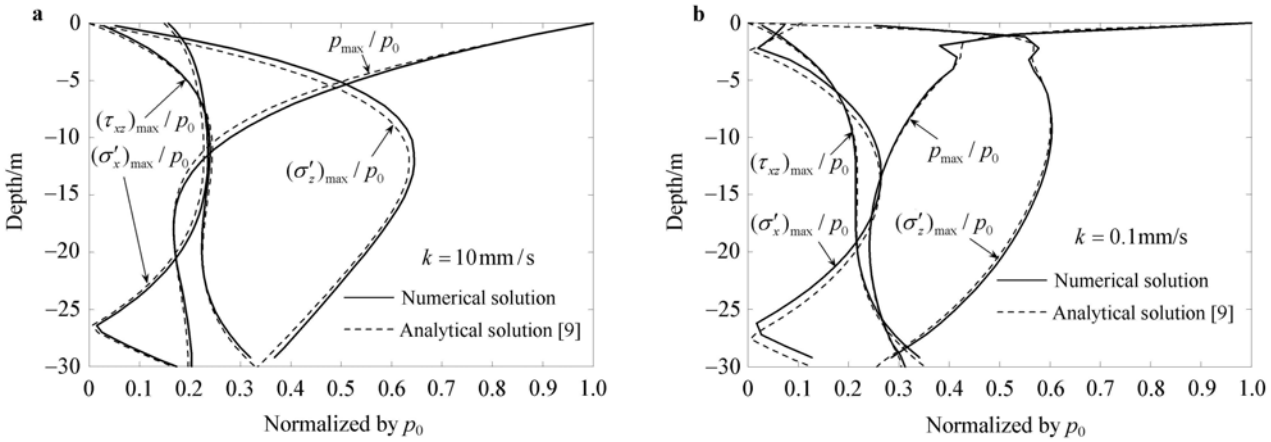

Fig. 4 Vertical distribution of the wave-induced soil response in **a** coarse sand and **b** fine sand ($T = 8.0$ s, $d = 20$ m, $L = 88.8$ m, $G = 10$ MPa, $\mu = 1/3$, $n = 0.2$, $S_r = 0.98$)

3.3.2 Comparison with the experimental data

Lu [31] conducted a series of lab experiments about the dynamic response of sand bed to the waves propagating on it in a wave flume which is 60 m long, 1.5 m wide and 1.8 m high (Fig. 5a). The waves generated in the wave flume include regular waves and cnoidal waves. The sand bed is consisted of coarse sand. The pore pressure at the four points on the midline of sand bed are monitored in experiments.

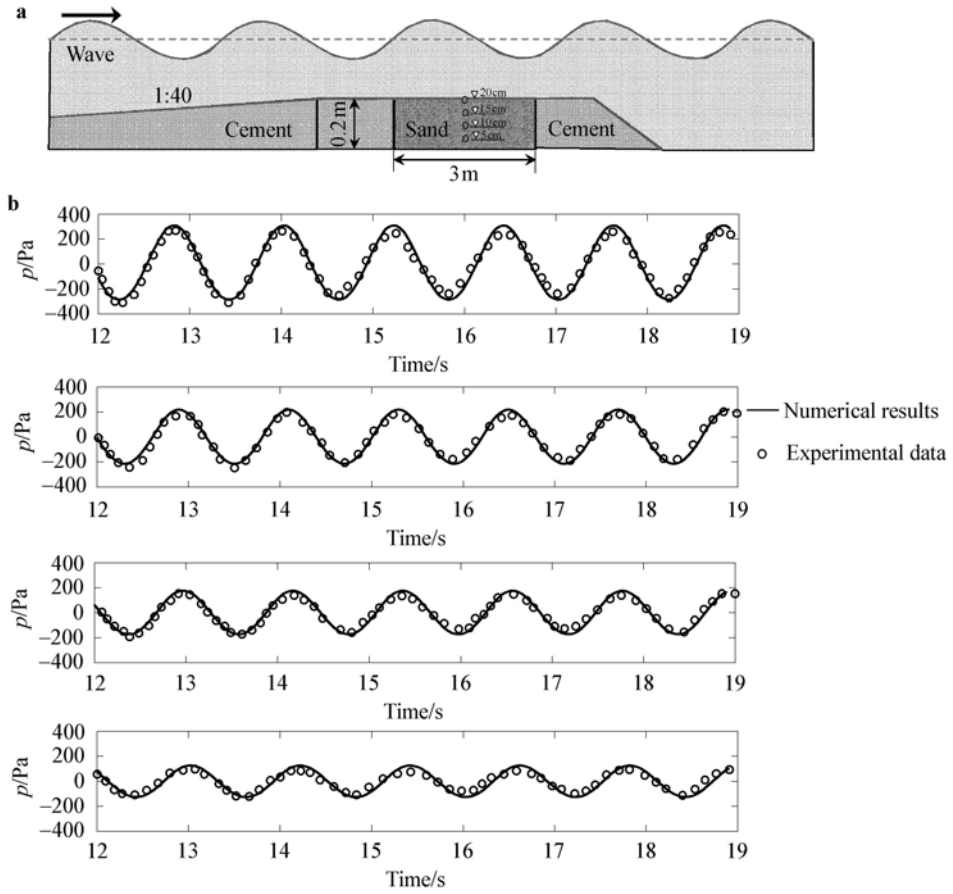

Fig. 5 **a** The experimental setup in Lu's tests [31]; **b** Comparisons of wave-induced dynamic pore pressure on the midline of sand bed

The properties of coarse sand provided by Lu [31] are: shear modulus $G = 10$ MPa, Possion's ratio $\mu = 0.3$, permeability $k = 1$ mm/s, porosity $n = 0.389\,3$, the mean size of sand particles $d_{50} = 0.44$ mm and saturation $S_r = 98\%$. The wave characteristics of the regular wave and cnoidal wave are $H = 12$ cm, $d = 0.4$ m, $T = 1.2$ s and $H = 12$ cm, $d = 0.3$ m, $T = 2.0$ s.

The comparisons of the regular wave induced dynamic pore pressure at the four points on the midline of sand bed between the numerical results and the experimental data are shown in Fig. 5b. As illustrated in Fig. 5b, the numerical results predicted by the numerical model developed could agree well with experimental data provided by Lu [31].

4 Results and discussions

In this section, we first discuss the effects of wave nonlinearity on the seabed response, based on the second-order Stokes wave theory. Second, we examine the influence of bottom shear stresses with the ratio of amplitudes of shear stresses to the dynamic wave pressures. Finally, a parametric study is presented to examine the effects of wave and soil characteristics on the seabed response.

4.1 Effects of wave nonlinearity

It is well known that the first-order linear wave is an approximation of the periodic wave with small amplitude in deep water. For the waves with large amplitude in shallow water, the linear wave theory is inadequate to describe them. The high order wave theory should be adopted. The valid range for 1st to 5th order wave can be found in Ref. [32]. In this part, the effect of the nonlinearity of wave on the seabed response under wave applying is checked for the large wave propagating in relative shallow water, for example $H = 3.0$ m, $d = 10.0$ m and $T = 8.0$ s.

The elevation of free surface of the linear wave and second order wave, and the induced pressure acting on seabed are examined first. Based on the numerical calculations, it is found that the difference of wave height between the linear wave and the second-order wave is up to 18.5%; and the difference of the induced pressure acting on seabed is about 5.2%. Obviously, the effect of nonlinearity of wave is significant for the large wave in shallow water.

Figures 6a and 6b illustrate the distribution of the seabed response under linear wave and second-order wave. As shown in the figure, for large wave in shallow water, the linear wave theory underestimates the pore pressure in the

upper part of seabed, overestimates the σ'_z in the middle part of seabed, and underestimates the σ'_x in the middle part of seabed. However, the shear stress τ_{xz} in seabed is not affected by the nonlinearity of wave. Overall, the effect of nonlinearity for large wave in shallow water is significant.

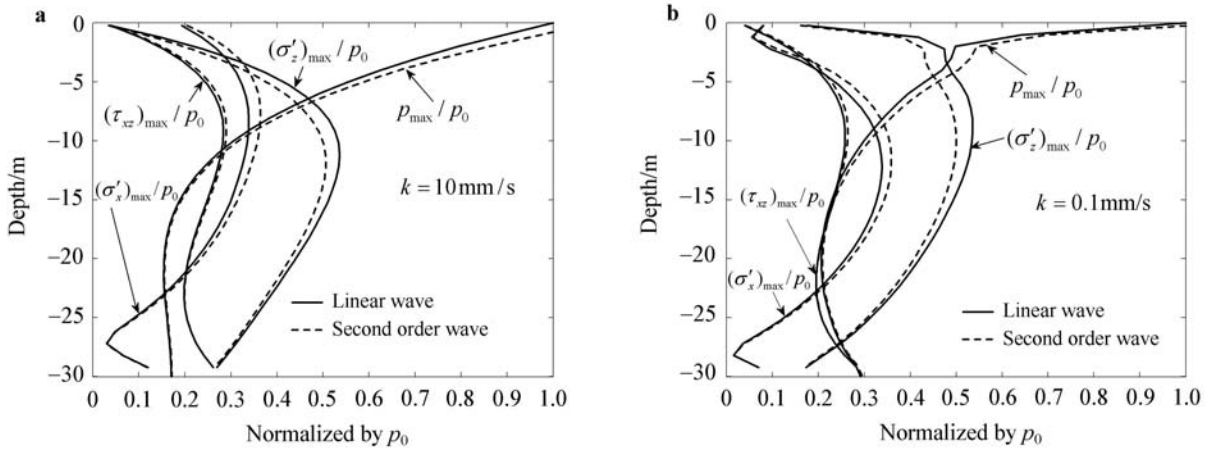

Fig. 6 The distribution of the seabed response induced by wave and bottom shear stress under linear wave and the second-order stokes wave ($T = 8.0$ s, $d = 10$ m, $H = 3.0$ m, $G = 10$ MPa, $\mu = 1/3$, $n = 0.3$, $S_r = 0.98$). **a** Coarse sand; **b** Fine sand

4.2 Effect of the amplitude of the bottom shear stresses (τ_0)

From the physical point of view, the bottom shear stress acting on seabed attributes to the viscosity of sea water, and the velocity gradient of sea water at the surface of seabed. Generally, the boundary layer theory are widely adopted to estimate the bottom shear stress. According to the boundary layer theory, the greater the velocity gradient at the surface of seabed, the greater the bottom shear stress acting on seabed. To simplify the problem, we only use the linear wave theory in this comparison. The dynamic wave pressure and bottom shear stresses can be simplified as

$$\begin{aligned} p_b(x,t) &= \frac{\rho g H}{2\cosh(kd)}\cos(kx-\omega t) \\ &= p_0\cos(kx-\omega t), \\ \tau_b(x,t) &= \frac{\sqrt{2}\beta_0\rho\nu k H}{2\delta}\cos\left(kx-\omega t-\frac{\pi}{4}\right) \\ &= \tau_0\cos\left(kx-\omega t-\frac{\pi}{4}\right). \end{aligned} \tag{47}$$

From Eq. (47), it is known that the bottom shear stress is positively proportional to the velocity magnitude at the top of boundary layer. For deep water, due to that the effect of wave could basically disappear at the surface of seabed, and the horizontal velocity of water particles in boundary layer is nearly 0. Therefore, the bottom shear stress is negligible. However, in the shallow water, the effect of wave is great on the surface of seabed, the horizontal velocity of water particles in boundary layer is considerable. The friction between the sea water and seabed can not be ignored. Additionally, the current always co-exists with the ocean wave in real ocean environment. The velocity of current generally is much greater than the wave-induced water particles velocity. This current will make the horizontal velocity of water particles in boundary layer increase greatly. It will further result in the great increase of the bottom shear stress acting on seabed. Unfortunately, little attempt has been made to develop a theory to estimate the bottom shear stress considering effect of current on boundary layer, and the interaction between the wave and current. Equation (47) does not consider the effect of current. Therefore, the bottom shear stress frequently is underestimated by Eq. (47) due to the existence of current in ocean environment. The theory considering the effect of current on boundary layer, and the interaction between the wave and current will be developed to accurately determine the bottom shear stress acting on seabed based on the boundary layer theory in the future.

To have a general understanding of the effects of τ_0, the magnitude of the bottom shear stress acting on the seabed (τ_0) is temporarily assumed as 1%, 5%, 10%, 15% of the dynamic pressure acting on the seabed (p_0). With the wave and soil conditions given in the Table 1, we attempt to find out the difference between the models with/without bottom shear stresses. Figure 7 clearly demonstrates the considerable effects of bottom shear stresses on the wave-induced seabed response. For example, if the bottom shear stresses are included, the maximum value of effective stresses σ'_z, σ'_x and τ_{xz} will become less than that without shear stresses ($\tau_0 = 0$) in the upper section of seabed. However, the wave-induced pore pressure will become greater in the whole seabed. For the σ'_z, the difference between two models is relatively small. It is noted that if the bottom shear stress is considered, the shear stress in the region near the surface of seabed is much greater.

The above numerical results ($\tau_0/p_0 = 10\%$) demonstrate the considerable effects of the bottom shear stress on the wave-induced seabed response. It is of interest to further examine the influence of the bottom shear stress amplitudes on the relative differences between two models.

As illustrated in Figs. 8 and 9, the greater the bottom shear stress, the more significant the effect on the wave-induced seabed response is observed. In addition, the inclusion of bottom shear stress has the most significant effect on the σ'_x and τ_{xz}. For example, the maximum difference of σ'_x

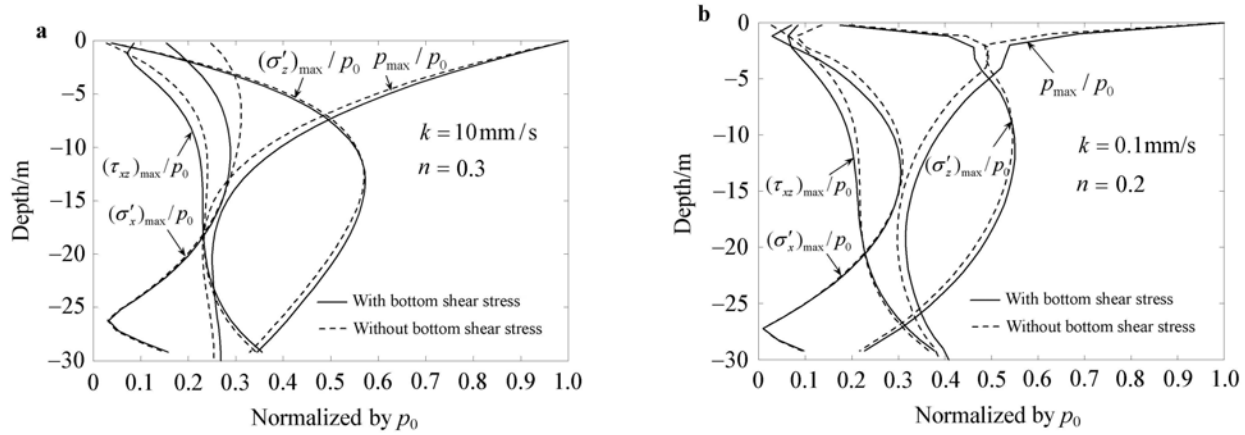

Fig. 7 Vertical distributions of wave-induced seabed response in **a** coarse sand and **b** fine sand ($T = 8.0$ s, $d = 20$ m, $G = 10$ MPa, $\mu = 1/3$, $S_r = 0.98$, $\tau_0/p_0 = 10\%$)

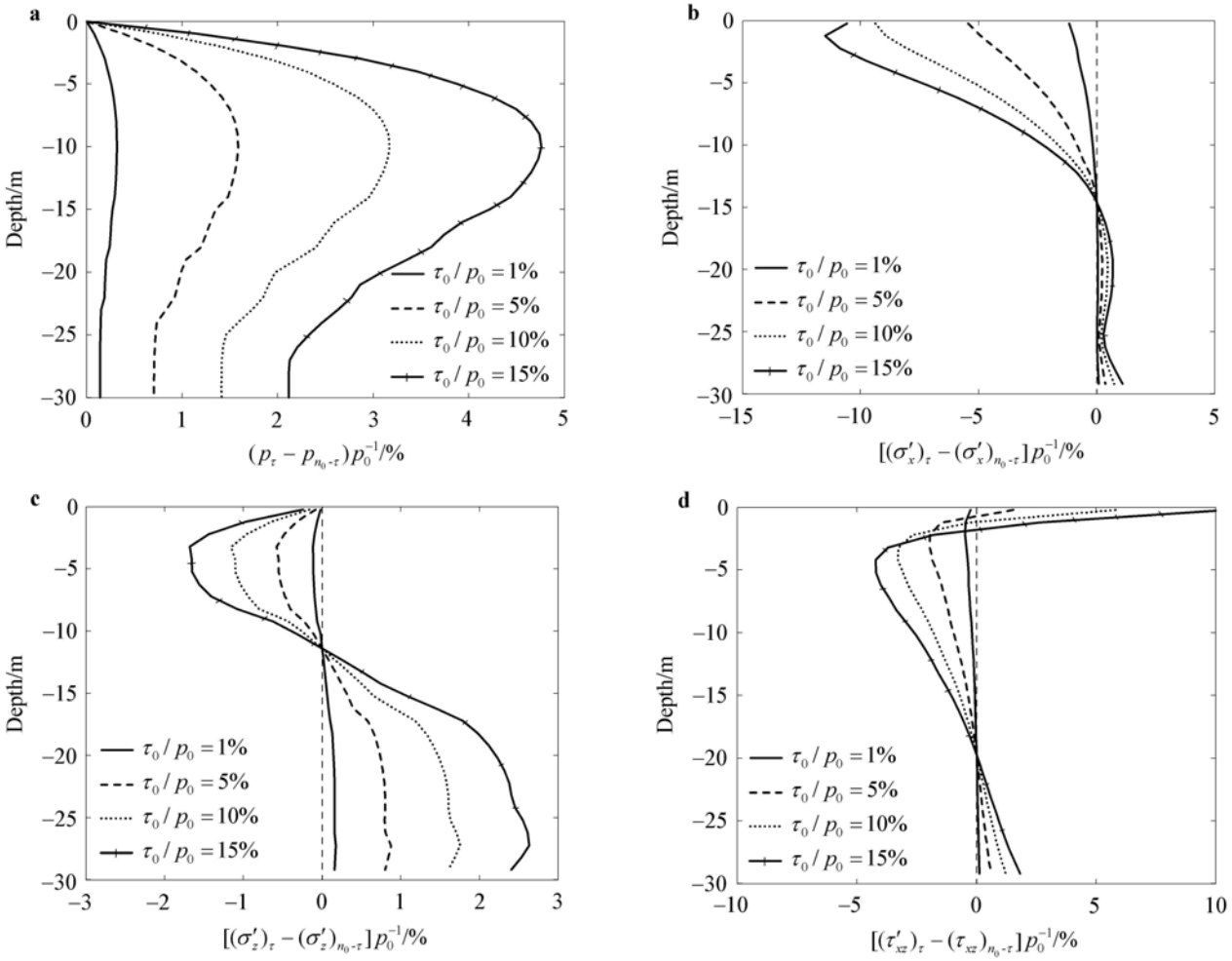

Fig. 8 Vertical distributions of the relative differences of wave-induced seabed response in coarse sand for various τ_0/p_0

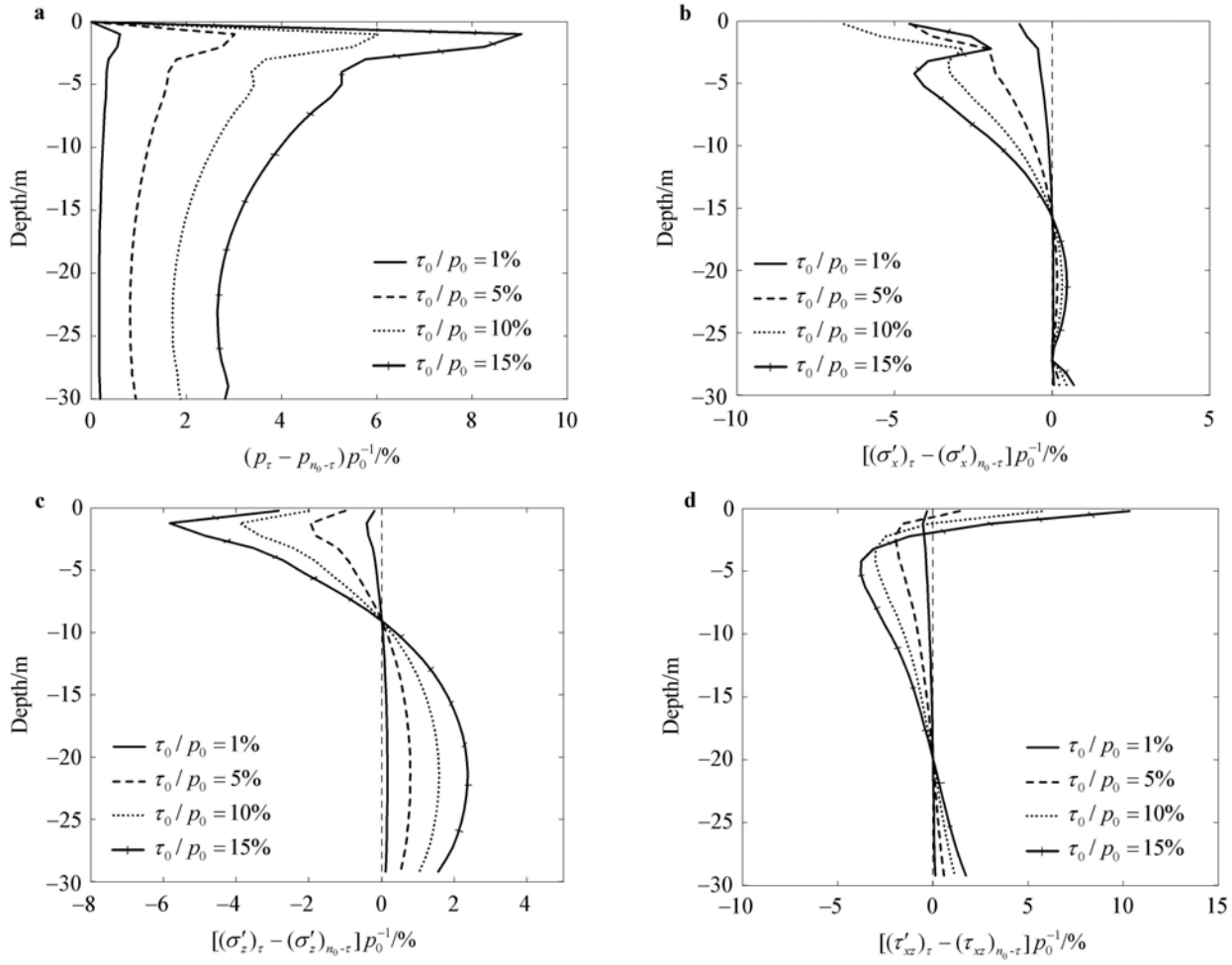

Fig. 9 Vertical distributions of the relative differences of wave-induced seabed response in fine sand for various τ_0/p_0

and τ_{xz} can reach up to 10% and 4.5% of p_0 in coarse sand, and 7.5% and 10% of p_0 in fine sand at the surface of seabed when $\tau_0/p_0 = 10\%$. On the other hand, the effects of bottom shear stress on σ'_z and pore pressure p are also visible (around 5%–10% of p_0). Comparing the relative differences shown in Figs. 8 and 9, it is found that the bottom shear stress has more significant effect on the σ'_x and τ_{xz} both in coarse sand and fine sand. However, the effect on pore pressure and σ'_z are more significant in fine sand than coarse sand. It is interesting to note that the effect of bottom shear stress on the σ'_x near the seabed surface in fine sand becomes less significant when the $\tau_0/p_0 = 15\%$ relative to situation in which $\tau_0/p_0 = 10\%$. This unusual results need to be further investigated in the future to see if the seabed instability occurs or not in the regions or other causes.

4.3 Parametric studies

4.3.1 Effects of wave characteristics

Basically, wave periods, water depths and wave heights are three essential wave parameters. Since we consider linear waves only, the effects of wave heights will be excluded as the results are presented in the non-dimensional form with p_0. Therefore, we only examine the effects of wave periods and water depths. Figure 10 presents the relative differences of wave-induced pore pressure in coarse and fine sand for various wave periods. As shown in the figures,the effect of the bottom shear stress become more significant as the wave period increases, especially in the region near the surface of seabed in fine sand. In general, a long period wave has more potential to generate more energy than a short one with the same wave height and water depth. Therefore, the dynamic pressure and the bottom shear stresses induced by a long period wave are greater than those by a short one. This may explain why the effect of bottom shear stresses induced by long period wave is greater than those by a short one.

Figure 11 illustrates the relative difference of wave-induced pore pressure for various water depths. The figure clearly indicates that the effect of bottom shear stress on the pore pressure increases as the water depth increases in both coarse sand and fine sand. However, overall, the influence of water depth on the pore pressure when the bottom shear stress is considered is relatively insignificant, compared with the wave periods.

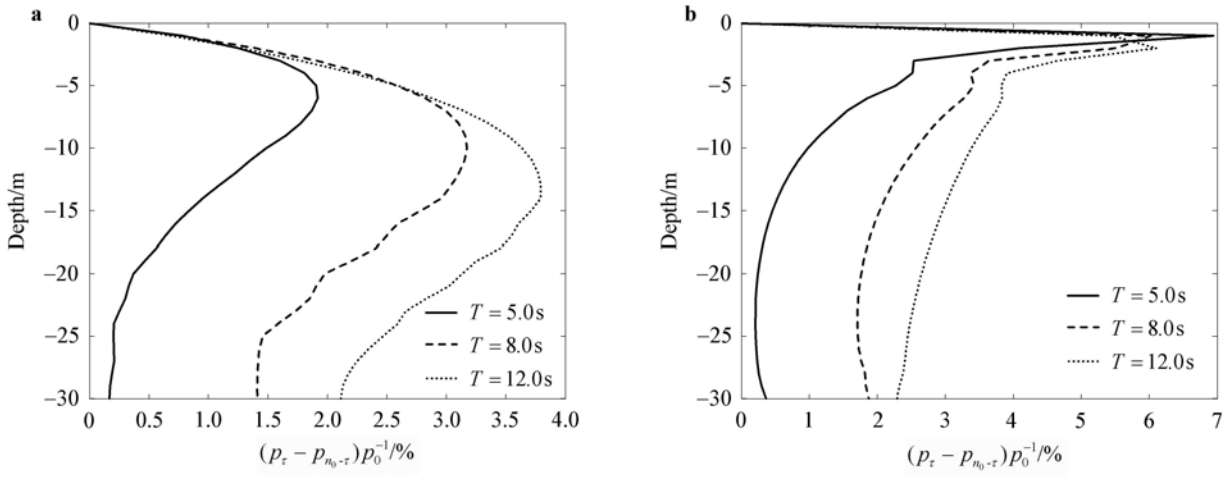

Fig. 10 Vertical distributions of the relative differences of wave-induced seabed response in coarse and fine sand for various wave periods. **a** Coarse sand; **b** Fine sand

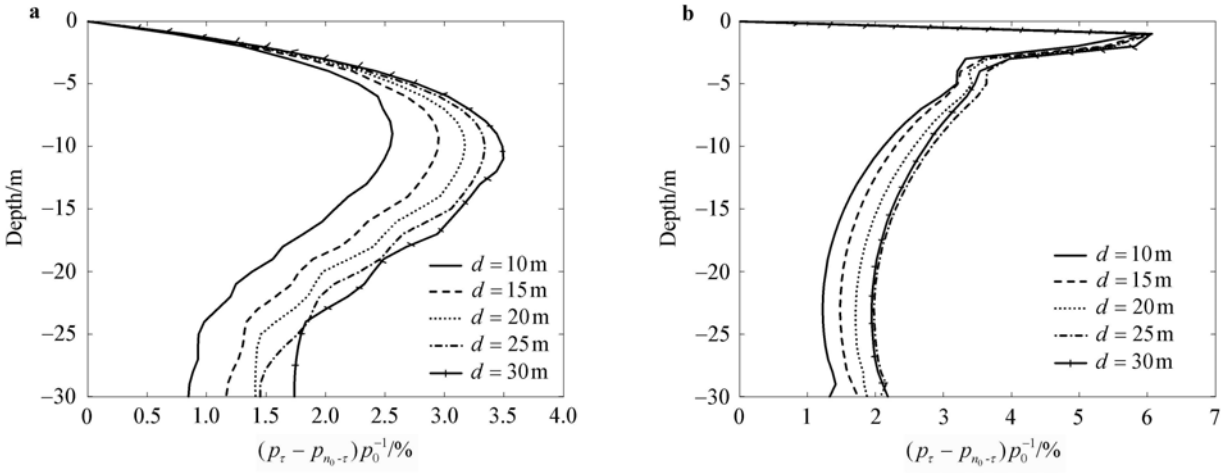

Fig. 11 Vertical distributions of the relative differences of wave-induced seabed response in coarse and fine sand for various water depth

4.3.2 Effects of soil characteristics

As report in the previous study [9], several soil properties significantly affect the evaluation of the wave-induced seabed response, i.e., the degree of saturation, seabed thickness and soil type. In this section, we will examine how these soil properties affect the influences of bottom shear stresses on the wave-induced seabed response variables. It has been reported that the seabed soil is a porous medium consisting of soil particles, pore water and trapped air bubbles [33,34]. It is also reported that the degree of saturation will significantly affect the wave-induced oscillatory soil response [9].

The relative differences of the wave-induced pore pressure in coarse and fine sand for various degrees of saturations are illustrated in Fig. 12. It is found that the degree of saturation has considerable effects on the wave-induced pore pressure when the bottom shear stresses are considered, especially in a fully saturated seabed. For example, the maximum relative difference could up to 7.5% of p_0.

It has been well known that a higher degree of saturation of soil means there is more pore water occuping the void in porous medium, which is beneficial to transmit the dynamic pressure or other effect from surface to bottom of seabed. Therefore, the effect of bottom shear stresses acting on seabed is most significant in fully saturated sand, and its effect will decrease as the degree of saturation decreases. An obvious difference between coarse sand and fine sand is the different permeabilities. For fine sand, the permeability is relatively small. It is difficult for the dynamic pressure to transmit from surface to bottom of seabed. Therefore, the effect of bottom shear stresses is more significant at the region near the seabed surface.

The thickness of a seabed is an another important factor that affects the dynamic response of a porous seabed under wave loading. Figure 13 shows that the effect of bottom shear stress at the top of seabed is almost identical with various seabed thicknesses. Near the bottom of seabed, the effect of bottom shear stress is more significant for thin seabed. Additionally, the effect of bottom shear stress is much more significant at the region near the surface of seabed in fine sand than in coarse sand.

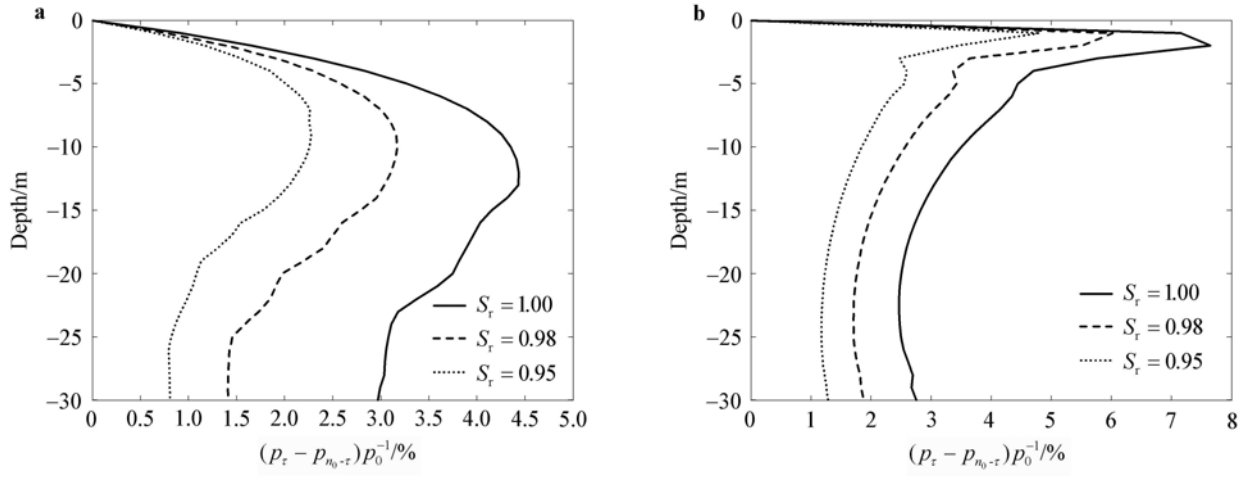

Fig. 12 Vertical distributions of the relative differences of wave-induced seabed response in coarse and fine sand for varisou degrees of saturations. **a** Coarse sand; **b** Fine sand

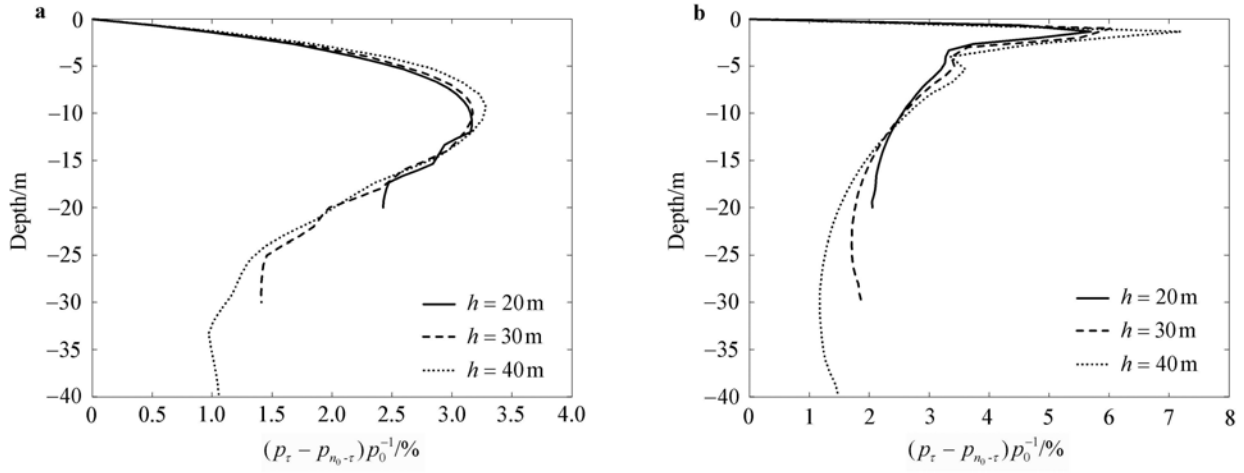

Fig. 13 Vertical distributions of the relative differences of wave-induced seabed response in coarse and fine sand for various seabed thicknesses. **a** Coarse sand; **b** Fine sand

5 Conclusions

In this study, the effects of bottom shear stress on the wave-induced dynamic response of a porous seabed are examined. The FEM model (SWANDYE-II) was adopted for the wave loading and bottom shear stresses are included in the previous PORO-WSSI model and form PORO-WSSI (shear) model. The numerical model has been verified with the analytical solution for the case without bottom shear stress, and the experimental data obtained from wave flume test (the bottom shear stress is included). Based on the numerical results presented, the following conclusions can be drawn:

(1) Based on the numerical examples, it is found that effective stresses (σ'_z and σ'_x) and shear stress (τ_{xz}) will be over-estimated if the bottom shear stress along the seabed surface is ignored. On the other hand, the pore water pressure will be under-estimated by the previous model without bottom shear stresses.

(2) The maximum relative difference of seabed response predicted by the models with and without bottom shear stresses could up of 10% for the condition $\tau_0/p_0 = 15\%$.

(3) Among wave properties, the wave period has more significant influences on the relative difference of seabed response between the models with and without bottom shear stresses.

(4) For soil properties, the degree of saturation has more influences on the relative difference, compared with seabed thickness. In general, the relative differences of seabed response are more significant in fine sand than in coarse sand.

In this study, we only consider linear wave loading with bottom shear stresses. For the non-linear wave loading with structure or more complicated wave-seabed-structure interaction system, it will be further investigated in the future study.

Acknowledgements Authors are grateful to Professor Andrew Chan at University of Birmingham for the sources code of SWANDYNE-II. This study is supported by State Key Laboratory of Ocean Engineering Self-Development (GKZD010053-3) and EPSRC (EP/G006482/1).

References

1 Chung, S.G., Kim, S.K., Kang, Y.J., et al: Failure of a breakwater founded on a thick normally consolidated clay layer. Géotechnique **56**(3), 393–409 (2006)
2 Lundgren, H., Lindhardt, J.H.C., Romold, C.J.: Stability of breakwaters on porous foundation. In: Proceeding of 12th International Conference on Soil Mechanics and Foundation Engineering, **1**, 451–454 (1989)
3 Silvester, R., Hsu, J.R.C.: Sines revisited. Journal of Waterway, Port, Coastal, Ocean Engineering, ASCE **115**(3), 327–344 (1989)
4 Zen, K., Umehara, Y., Finn, W.D.L.: A case study of the wave-induced liquefaction of sand layers under damaged breakwater. In: Proceeding 3rd Canadian Conference on Marine Geotechnical Engineering, 505–520 (1985)
5 Zhang, F.G., Ge, Z.J.: A study on some causes of rubble mound breakwater failure. China Ocean Engineering **10**(4), 473–481 (1996)
6 Biot, M.A.: General theory of three-dimensional consolidation. Journal of Applied Physics **26**(2), 155–164 (1941)
7 Biot, M.A.: Theory of propagation of elastic waves in a fluid-saturated porous solid. Part I: Low frequency range. Journal of Acoustical Society of America **28**(20), 168–177 (1956)
8 Yamamoto, T., Koning, H., Sellmeijer, H., et al.: On the response of a poro-elastic bed to water waves. Journal of Fluid Mechanics **87**(1), 193–206 (1978)
9 Hsu, J.R.C., Jeng, D.S.: Wave-induced soil response in an unsaturated anisotropic seabed of finite thickness. International Journal for Numerical and Analytical Methods in Geomechanics **18**(11), 785–807 (1994)
10 Hsu, J.R.C., Jeng, D.S., Lee, C.P.: Oscillatory soil response and liquefaction in an unsaturated layered seabed. International Journal for Numerical and Analytical Methods in Geomechanics **19**(12), 825–849 (1995)
11 Jeng, D.S., Lin, Y.S.: Finite element modelling for water waves– soil interaction. Soil Dynamics and Earthquake Engineering **15**(5), 283–300 (1996)
12 Jeng, D.S., Seymour, B.R.: Response in seabed of finite depth with variable permeability. Journal of Geotechnical and Geoenvironmental Engineering, ASCE **123**(10), 902–911 (1997)
13 Seymour, B.R., Jeng, D.S., Hsu, J.R.C.: Transient soil response in a porous seabed with variable permeability. Ocean Engineering **23**(1), 27–46 (1996)
14 Jeng, D.S.: Soil response in cross-anisotropic seabed due to standing waves. Journal of Geotechnical and Geoenvironmental Engineering, ASCE **123**(1), 9–19 (1997)
15 Jeng, D.S., Lin, Y.S.: Non-linear wave-induced response of porous seabed: A finite element analysis. International Journal for Numerical and Analytical Methods in Geomechanics **21**(1), 15–42 (1997)
16 Jeng, D.S.: Wave-induced sea floor dynamics. Applied Mechanics Reviews **56**(4), 407–429 (2003)
17 Zhou, X.L., Xu, B., Wang, J.H., et al..: An analytical solution for wave-induced seabed response in a multi-layered poro-elastic seabed. Ocean Engineering **38**(1), 119–129 (2011)
18 Sakai, T., Hattori, A., Hatanaka, K.: Wave-induced transient porewater pressure and seabed instability in the surf zone. In: Proceeding of International Conference on Geotechnical Engineering for Coastal Development-Theory and Practice on soft Ground, **1**, 627–632. Yokohama, Japan (1991)
19 Jonsson, I.G.: A new approach to oscillatory rough turbulent boundary layers. Ocean Engineering **7**(1), 109–152 (1980)
20 Jeng, D.S.: Wave-induced seabed response in front of a breakwater. [Ph.D. Thesis], University of Western Australia (1997)
21 Zienkiewicz, O.C., Chang, C.T., Bettess, P.: Drained, undrained, consolidating and dynamic behaviour assumptions in soils. GGéotechnique **30**(4), 385–395 (1980)
22 Jeng, D.S., Cha, D.H.: Effects of dynamic soil behavior and wave non-linearity on the wave-induced pore pressure and effective stresses in porous seabed. Ocean Engineering **30**(16), 2065–2089 (2003)
23 Ulker, M.B.C., Rahman, M.S., Jeng, D.S.:Wave-induced response of seabed: Various formulations and their applicability. Applied Ocean Research **31**(1), 12–24 (2009)
24 Chan, A.H.C.: A unified finite element solution to static and dynamic problems of geomechanics. [Ph.D. Thesis], University of Wales, Swansea Wales (1988)
25 Zienkiewicz, O.C., Chan, A.H.C., Pastor, M., et al.: Computational Geomechanics with Special Reference to Earthquake Engineering. John Wiley and Sons, England (1999)
26 Jeng, D.S.: Porous model for wave-seabed-structure interaction. Tech. Rep. R2010-1, Division of Civil Engineering, University of Dundee, UK, available online at http://www.personal.dundee.ac.uk/d̃jeng/report.htm (2010)
27 Tsai, C.P.: Laminer boundary layer flows under the action of waves in front of a breakwater. Journal of the Chinese Institute of Civil and Hydraulic Engineering **6**(4), 433–443 (1994)
28 Zienkiewicz, O.C., Scott, F.C.: On the principle of repeatability and its application in analysis of turbine and pump impellers. International Journal for Numerical Methods in Engineering **9**, 445–452 (1972)
29 Katona, M.G., Zienkiewicz, O.C.: A unified set of single step algorithms. Part 3: The beta-m method, a generalisation of the Newmark scheme. Int. J. Numer. Methods Eng. **21**, 1345–1359 (1985)
30 Newmark, N.M.: A method of computation for structural dynamics. Journal of Engineering Mechanics Division, ASCE **85**(1), 67–94 (1959)
31 Lu, H.B.: The research on pore water pressure response to waves in sandy seabed. [Ph.D. Thesis], Changsha University of Science & Technology, Changsha Hunan China (2005)
32 Méhauté, B.L.: Introduction to Hydrodynamics and Water Waves. Springer-Verlag, New York (1976)
33 Esrig, M.I., Kirby, R.C.: Implication of gas content for predicting the stability of submarine slopes. Marine Geotechnology **2**(1), 81–100 (1977)
34 Pietruszczak, S., Pande, G.N.: Constitutive relations for partially saturated soils containing gas inclusions. Journal of Geotechnical Engineering, ASCE **122**(1), 50–59 (1996)